Collective Stopping and Ion Heating in Relativistic-Electron-Beam Transport for Fast Ignition

M. Honda, J. Meyer-ter-Vehn,* and A. Pukhov†

Max-Planck-Institut für Quantenoptik, Hans-Kopfermann-Strasse 1, D-85748 Garching, Germany

(Received 1 March 2000)

Filamented transport of laser-generated relativistic electron beams in a plasma is studied with reference to fast ignition of fusion targets. The study is based on transverse two-dimensional particle-in-cell simulation. Coalescence of current filaments and related ion dynamics are found to determine beam stopping and ion heating.

PACS numbers: 52.40.Mj, 52.35.Qz, 52.65.Rr

High intensity laser pulses of 10^{20} W/cm^2 and more are now available [1] to drive relativistic electron currents of the order of 100 kA and more into dense plasma, creating up to gigagauss magnetic fields [2]. Plans exist to use such pulses for fast ignition (FI) of inertial confinement fusion (ICF) targets, expected to reduce ignition requirements significantly [3]. For fast ignition, the ignitor pulse has to be transported to the compressed fusion fuel through highly overdense plasma. It is envisioned that the laser pulse first propagates through a self-drilled hole into the plasma corona, but that the final transport has to be carried by electrons [4]. Transporting a petawatt (10^{15} W) pulse, say by 10 MeV electrons, amounts to a current of 100 MA, far above the Alfvén limit of $I_A \simeq 17\ \mathrm{kA} \cdot \gamma$; here $\gamma m_e c^2$ is the energy of beam electrons. It has been realized that such currents can be transported only in the presence of compensating plasma currents to suppress the magnetic field [5–7].

This has significant consequences for the FI concept as a whole. They have not been discussed so far. We show that it may lead to collective beam stopping significantly larger than binary Coulomb stopping and a new mechanism of ion heating. Both effects should be observable experimentally. The underlying physics is also relevant to magnetic reconnection [8]. Collimated electron beams driven by high-intensity laser pulses have been observed recently in solid target material [9]; so far, beam parameters such as beam power and energy spectra were not measured and spatial resolution was insufficient to detect filamentary structures of the type discussed below.

The system of a beam and a compensating plasma current is subject to filamentation (Weibel) instability [10] and decays into current filaments on the time scale of the beam plasma frequency $\omega_b^{-1} = (4\pi e^2 n_b/m_e)^{-1/2}$, where n_b is the relativistic electron beam (REB) electron density. The nonlinear dynamics of these filaments have been studied in [11] and more recently in [12], including movable ions. One finds that the compensating plasma currents are expelled from the relativistic beam volumes and coaxial filamentary structures self-organize with a pinching beam in the center and a return current sheath expanding radially outwards.

In the following, we concentrate on the residual magnetic interaction between the filaments which causes these coaxial structures to attract each other and to merge in violent events of coalescence. Each coalescence dissipates a sizable fraction of the directed beam energy into transverse electron heating and magnetic field. The major point of this Letter is that this dissipation represents a collective mechanism of beam stopping which is much larger than the classical stopping, at least for moderate ratios of initial plasma/beam densities n_0/n_b. For n_b equal to the critical density $n_c = \pi m_e c^2/e^2\lambda_L^2$ (λ_L laser wavelength) and $n_0/n_b = 10$, we find effective stopping powers a factor of 100–1000 larger than due to classical stopping. This may be needed for FI. Recent studies have shown [13] that beam electrons produced at FI irradiances of 10^{20} W/cm^2 have energies of 10–100 MeV rather than the 1–10 MeV originally expected [3]. They would not be stopped in the ignition spot unless there is additional energy loss.

Of course, the FI configuration involves a plasma density with a steep gradient, rising from n_c at the end of the laser channel to $10^5 n_c$ in the fuel core, and n_0/n_b rises accordingly. Concerning beam energy loss under these conditions, Deutsch *et al.* [14] have argued that it occurs essentially as classical stopping due to the large value of $n_p/n_b \approx 10^5$ at core density. Here we question this position in view of the transverse structuring of the current pattern occurring in the layers of intermediate density. Below we demonstrate that the current filamentation perforates the ion density distribution, and we conjecture that a system of current pipes with small diameters of a few debye lengths [7] [in the order of $k_p^{-1} = (4\pi e^2 n_p/m_e c^2)^{-1/2} \sim 1\text{–}100$ nm in transverse beam direction] will penetrate into deeper layers and influence energy deposition.

The full three-dimensional simulation of a 100 MA current with a cross section of $(45\ \mu\mathrm{m})^2$ propagating up to core density over time periods of 10–100 ps is out of our present computational capacities. Thus, we choose a two-dimensional particle-in-cell (2D-PIC) simulation with periodic boundary conditions in the plane transverse to beam propagation. We concentrate on the elementary processes occurring in this model configuration. The

 0031-9007/00/85(10)/2128(4)$15.00

simulation domain we can afford is $S = 12.7 \times 12.7/k_p^2$, or $(0.63\ \mu\text{m})^2$, with 20 kA initial current flowing through it. This is only a small fraction of the total fast ignitor beam. Still, it is representative for the physics discussed below, as it is many plasma skin depths wide and the initial current is close to the Alfvén limit.

The simulation starts with a uniform plasma density of $n_0 = 1.1 \times 10^{22}\ \text{cm}^{-3} = 10 n_c$, where n_c is the critical density of $\lambda_L = 1\ \mu$m light, and a beam density of $n_b/n_0 = 0.1$. This implies $\omega_p = 5.96\ \text{fs}^{-1}$ and $k_p = 19.9\ \mu\text{m}^{-1}$. Beam electrons are chosen to have an energy of $\gamma_0 = 2.5$ and a thermal spread of $v_{\text{th}}/c \approx 10^{-4}$. Initially, the beam current is completely compensated by a plasma return current. In this configuration we observe about 100 filaments emerging immediately after the initial decay phase [12]. Discussion in the present paper concentrates on the coalescence process in the nonlinear stage when only a few filaments are left in the simulation square. The code VLPL [15] is used for the simulation, involving both 39 040 electrons and protons with mass $m_i = 1836 m_e$. It is supplemented by a relativistic collision package [12]. However, one should notice that, for the filamentation and coalescence dynamics studied here, collisions play a minor role. For the thermal collision frequency ν_c relevant for the return currents, one finds $\nu_c/\omega_p \ll 1$ up to the highest densities.

The temporal evolution of the forward (z direction) electron power flux $\Phi_+ = -\sum_{v_z<0} m_e c^2 \langle(\gamma - 1) n_e v_z\rangle$ is shown in Fig. 1. The heavy curve corresponds to the full simulation including ion motion. One should notice that already after $\omega_p t = 200$, corresponding to 30 fs and a beam propagation distance of $ct \approx 10\ \mu$m, the beam power has fallen by 40%–50%. This implies an effective stopping range in the order of 10^{-4} g/cm^2 and should be compared with the classical Coulomb range of 0.5 g/cm^2 for $\gamma_0 = 2.5$ electrons, as given in [3]. Apparently, the stopping mechanism in the present situation is quite different from that of binary Coulomb collisions.

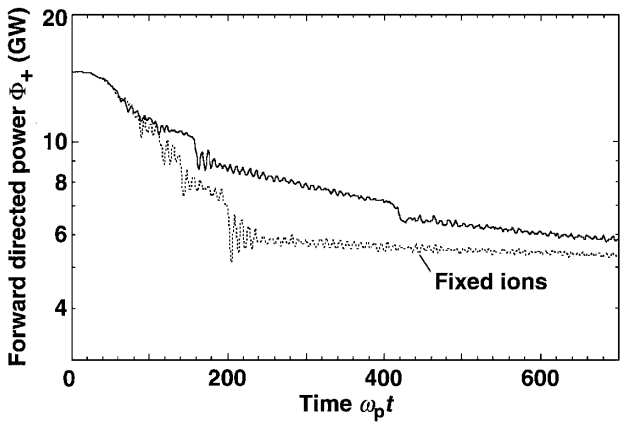

FIG. 1. Temporal evolution of forward-directed electron beam power for full simulation including ion motion (heavy curve) and for ions kept fixed (light curve). Collisional effects are included in both cases.

In Fig. 1 no beam stopping is observed in the first period up to $\omega_p t = 25$, which coincides with the linear stage of the electromagnetic instability. The second, nonlinear stage begins when forward and return currents have separated spatially but still have a uniform ion background. The radius of the beam filament is then given by $(k_p R)^2 = 4\gamma I/I_A$, where the beam current I is normalized by the Alfvén current $I_A = \gamma m_e c^3/e$. Below we refer to R as the separatrix radius. An example of the current pattern which now evolves is shown in Fig. 2(a) for $\omega_p t = 120$. One observes four beam filaments (red spots), each surrounded by a return current sheath (bluish rings), which screens the magnetic field. Frames (a)–(d) of Fig. 2 display the temporal evolution. Filaments A and B in frame (a) attract each other and merge into filament AB of frame (b). This coalescence is related to a sudden drop of beam power by 15%, as seen in Fig. 1 at $\omega_p t = 160$. The corresponding energy is converted into magnetic field

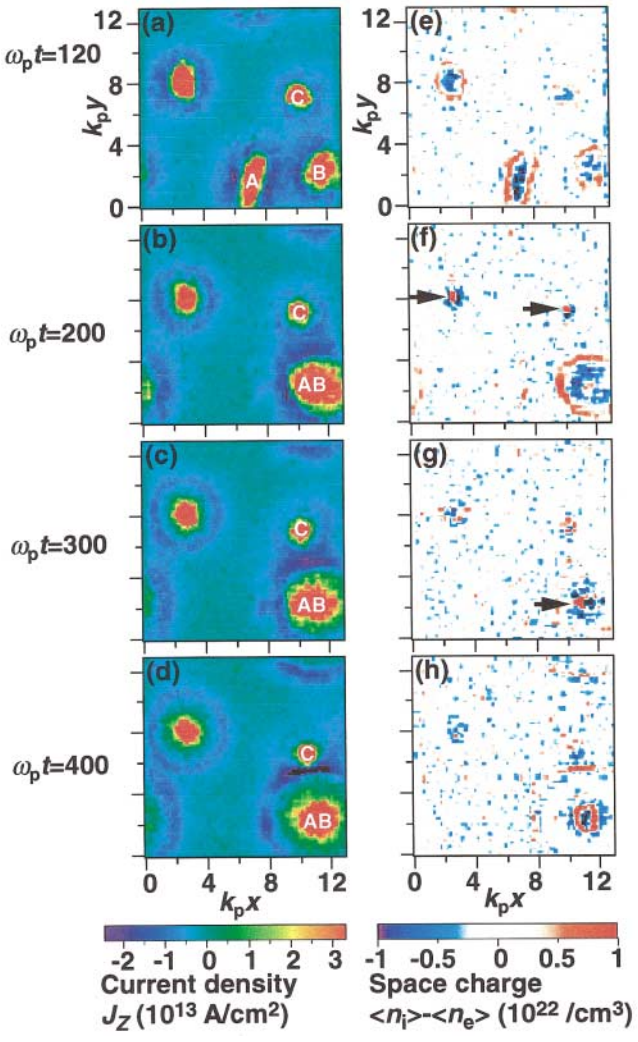

FIG. 2 (color). Left column: J_z current density plotted in transverse (x, y) plane for times given; right column: corresponding space charge density, given for times $\omega_p t = 120$ (a),(e), 200 (b),(f), 300 (c),(g), and 400 (d),(h). Arrows mark spots of imploded ion cores. For explanation, see text.

energy and transverse electron heat. The next step occurs at $\omega_p t = 420$ corresponding to the coalescence of filaments AB with C. The gradual decrease of beam power between the steps is correlated with the pinching of the filament cores and the cylindrical expansion of the return current sheaths seen in Figs. 2(b)–2(d), which both lead to an increase of magnetic energy.

It is instructive to look at the same current dynamics with ion background kept fixed. The collective beam stopping is then even more effective, as seen from the light curve in Fig. 1. The reason is that the transverse shifting of current filaments can then occur without ion inertia involved and may be described by pure electron magnetohydrodynamics [16]. We find the B_z evolution in the form of the Hasegawa-Mima equation [17,18]

$$\omega_p^2 \partial_t \left(B_z - \frac{1}{k_p^2} \Delta B_z \right) + \frac{1}{k_p^2} \frac{e}{mc^3} \nabla B_z \times \nabla \Delta B_z = 0 . \tag{1}$$

Here the stream function for the transverse electron fluid velocity conforms to $\mathbf{v}_\perp = -(c/4\pi en)\mathbf{e}_z \times \nabla B_z$ [19]. Although the "core" region of the filaments must be described kinetically, Eq. (1) is perfectly valid in the "mantle" region outside of the separatrix, where the cold return current flows. It is found that a filament moving with a transverse velocity $\mathbf{u}$ is represented by the dipole vortex solution of (1): $eB_z\mathbf{e}_z/mc\omega_p = (\mathbf{u} \times \mathbf{r}/c|r|)k_p R K_1(k_p r)/K_1(k_p R)$ for $r > R$ [18]. Here K_1 is a modified Bessel function. We see these vortices in the simulation when plotting B_z. Figure 3(a) gives an example for two filaments just before merging, seen in the current plot of Fig. 3(b) as the stretched current filament. As the filaments are moving toward each other, the polarities of the dipoles are opposite.

The time needed for filaments to coalesce can be estimated, taking the residual magnetic interaction in the form $B_0 \exp(-k_p r)$ at large distances r from a filament. The field strength is given by $eB_0/mc\omega_p \approx (\gamma I/I_A)^{1/2} \exp(k_p R)$. We then estimate the coalescence time τ as $(\omega_p \tau)^2 \approx (\gamma I_A/I)^{1/2} \exp(k_p d)$ for distances $d \gg R$ between the filaments.

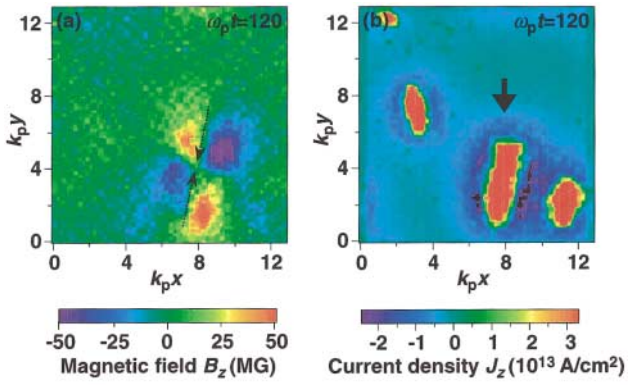

FIG. 3 (color). (a) B_z field related to electron vortices from a simulation with fixed ion background, plotted in transverse (x, y) plane for time $\omega_p t = 120$; (b) corresponding J_z current density distribution. The stretched current filament [marked by arrow in (b)] actually consists of two beam filaments just before merging; the dashed arrows in (a) indicate the drift velocities of these filaments.

With ion motion included, the dynamics changes after a few ion plasma periods, $\omega_i^{-1} = \sqrt{m_i/m_e}/\omega_p$. The magnetic field B of each individual filament exerts a magnetic pressure $P_B = B^2/8\pi$ on the surrounding plasma, up to 1 GBar for 160 MGauss. It depletes the ion density around the beam such that the beam gets trapped in the ion profile and any transverse displacement involves ion inertia. Therefore the time τ between coalescences becomes longer, as one observes in Fig. 1. The dominant mechanism of coalescence is now different. Because of the magnetic pressure, the return current sheaths expand radially with an expansion velocity $v_\perp$ that can be estimated by balancing the magnetic pressure P_B with the ion momentum transfer $n_i m_i v_\perp^2$. We get $v_\perp/c \approx eB/m_i c\omega_i \approx \sqrt{m_e/m_i}\,(2\gamma I/I_A)/(k_p R)$. The field energy grows with the void volume inside the separatrix at the expanse of beam power and accounts in part for the gradual beam stopping between coalescences. Filament coalescence occurs when the separatrices of neighboring filaments touch [see Fig. 2(d)] such that the unscreened cores start to see each other and merge.

Let us now have a closer look at ion dynamics inside filaments during and after a coalescence event. It is accompanied by strong charge separation ($n_i - n_e \sim 10^{22}$ cm^{-3}) as seen in Figs. 2(e) and 2(f). The red rings in frame (e) identify ion halos around pinching electron cores (blue), corresponding to the four filaments of frame (a). In frame (f) filaments A and B have merged into AB again showing the ion halo. The charge separation generates electrostatic fields of order $E_r \sim |\mathbf{v}_b \times \mathbf{B}|/c \sim 10^{10}$ V/cm. On a short time scale, this field balances the centripetal magnetic force acting on the beam electrons until the ions are accelerated radially inwards. After a while the imploding ions pile up in the center of the filament cores. This stage is seen as red dots (marked by arrows) in the space charge plots (f) and (g). The beam electrons are seen as blue clouds surrounding the dots. Apparently, their transverse temperature is too high to screen the ion charge piling up in the center. The third stage of ion motion shows up in the lower right corner of frame (h), where the ions are seen as a cylindrically expanding ring, representing a collisionless shock.

The dynamics of ion implosion is so violent that it may lead to neutron production in fusion fuel. This is illustrated in Fig. 4 in terms of the ion velocity distributions (β_y). It is plotted along the vertical cut at $k_p x = 11$ shown in the inset. At $\omega_p t = 300$ ions form a core centered at $k_p y = 2.3 \pm 0.3$ with a diverging velocity of $|\beta_d| \approx (4\text{–}5) \times 10^{-3}$ at its boundary, while outer ions still implode with a maximum velocity of $|\beta_c| \approx 8 \times 10^{-3}$. This distribution has changed drastically at $\omega_p t = 400$, now showing energetic ion "wings" with ion energies up to

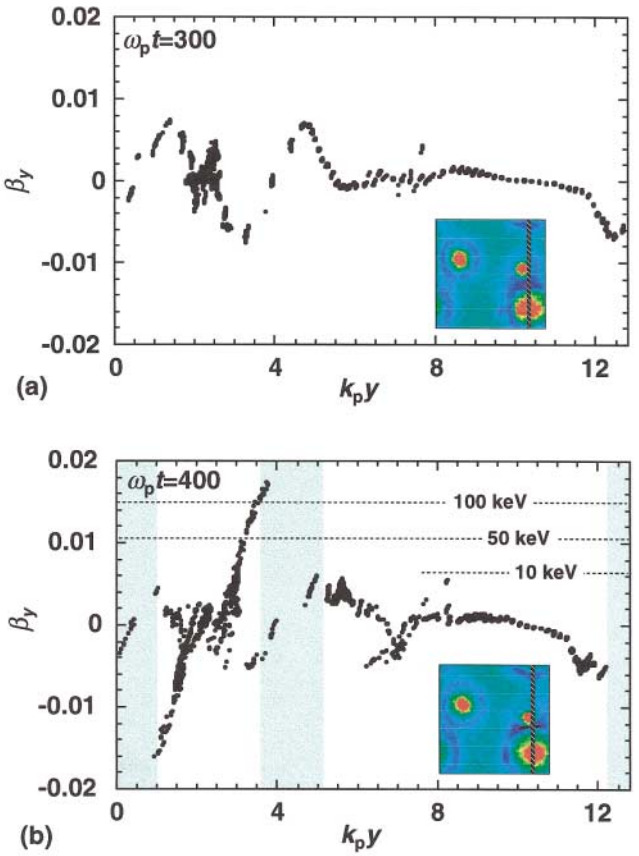

FIG. 4 (color). Ion velocity distribution (β_y) plotted along the cut in the y direction shown as a vertical bar in the color insets for (a) $\omega_p t = 300$ and (b) $\omega_p t = 400$. The green bands in (b) mark the region around the filament core which is practically void of plasma and only filled with magnetic field. The simulation is the same as for Figs. 1 and 2 with movable ions.

150 keV. The maximum velocity can be understood as bouncing of imploding ions on the electrostatic potential inherent to the collisionless shock of the expanding ion core [20], giving $\beta_{\max} = |\beta_c| + 2|\beta_d| \approx 0.016$–$0.018$. One may notice that similar ion acceleration occurs at the smaller filament, located at $k_p y = 7.2$ and leading to energies up to 10 keV. These ion energies are sufficient to produce fusion neutrons in a deuterium plasma. Besides ion acceleration in electrostatic fields directly produced by laser interaction, the pinch dynamics of current filaments is therefore still another mechanism which may contribute to the neutron production observed in recent experiments [21]. In the present simulation, the overall ion heating amounts to 3% of the total energy at $t = 100$ fs. The bulk of the dissipated energy goes in equal parts to magnetic field energy and transverse electron heating, leading to an isothermal equilibrium $\nabla B^2/8\pi \approx T_{b\perp} \nabla n_b$ with transverse temperature $T_{b\perp} \geq 100$ keV.

In conclusion, we have discussed elementary plasma processes in REB transport with large currents as encountered in the FI scenario. The important result is that filament coalescence and subsequent radial dynamics represent the major dissipative mechanism in this situation leading to strong collective stopping of the beam. The present study is restricted to 2D-PIC simulation and a plasma/beam density ratio of 10. In order to fully demonstrate the relevance of the present results to fast ignition, it needs to be extended to three dimensions and to density gradients rising up to ICF fuel density.

We acknowledge useful discussions with S. V. Bulanov, A. V. Kingsep, and H.-J. Kull. M. H. and A. P. thank the Max-Planck-Institut für Quantenoptik for its hospitality. This work was supported in part by EURATOM, by the Bundesministerium für Bildung und Forschung (Bonn), and by the Deutsche Forschungsgemeinschaft.

*Electronic address: meyer-ter-vehn@mpq.mpg.de
†Permanent address: Moscow Institute for Physics and Technology, Dolgoprudnyi, Moscow Region, Russia.

[1] D. Strickland and G. Mourou, Opt. Commun. **56**, 219 (1985).
[2] S. C. Wilks *et al.,* Phys. Rev. Lett. **69**, 1383 (1992); A. Pukhov and J. Meyer-ter-Vehn, Phys. Rev. Lett. **76**, 3975 (1996); Laser Part. Beams **17**, 571 (1999).
[3] M. Tabak *et al.,* Phys. Plasmas **1**, 1626 (1994).
[4] A. Pukhov and J. Meyer-ter-Vehn, Phys. Rev. Lett. **79**, 2686 (1997); Phys. Plasmas **5**, 1880 (1998).
[5] M. H. Key *et al.,* in *Proceedings of First Conference of Inertial Fusion Sciences and Applications, Bordeaux, France, 1999* (Elsevier, Paris, 2000).
[6] Y. Sentoku, K. Mima, S. Kojima, and H. Ruhl, Plasmas **7**, 689 (2000).
[7] M. Honda, Phys. Plasmas **7**, 1606 (2000).
[8] T. Tajima and K. Shibata, *Plasma Astrophysics* (Addison-Wesley, Reading, MA, 1996).
[9] M. Takarakis *et al.,* Phys. Rev. Lett. **81**, 999 (1998); M. Borghesi *et al.,* Phys. Rev. Lett. **83**, 4309 (1999); L. Gremillet *et al.,* Phys. Rev. Lett. **83**, 5015 (1999).
[10] E. S. Weibel, Phys. Rev. Lett. **2**, 83 (1959); F. Califano *et al.,* Phys. Rev. E **56**, 963 (1997); **57**, 7048 (1998); **58**, 7837 (1998).
[11] R. Lee and M. Lampe, Phys. Rev. Lett. **31**, 1390 (1973).
[12] M. Honda, J. Meyer-ter-Vehn, and A. Pukhov, Phys. Plasmas **7**, 1302 (2000).
[13] A. Pukhov, Z.-M. Sheng, and J. Meyer-ter-Vehn, Phys. Plasmas **6**, 2847 (1999).
[14] C. Deutsch *et al.,* Phys. Rev. Lett. **77**, 2483 (1996).
[15] A. Pukhov, J. Plasma Phys. **61**, 425 (1999).
[16] A. V. Kingsep, K. V. Chukbar, and V. V. Yankov, in *Reviews of Plasma Physics,* edited by B. B. Kadomtsev (Consulting Bureau, London, 1990), Vol. 16, p. 243.
[17] A. Hasegawa and K. Mima, Phys. Rev. Lett. **39**, 205 (1977).
[18] J. Nycander, V. P. Pavlenko, and L. Stenflo, Phys. Fluids **30**, 1367 (1987).
[19] C. Matsuoka and K. Nozaki, Phys. Fluids B **4**, 551 (1992).
[20] J. Denavit, Phys. Rev. Lett. **69**, 3052 (1992).
[21] A. P. Fews *et al.,* Phys. Rev. Lett. **73**, 1801 (1994); P. A. Norreys *et al.,* Plasma Phys. Controlled Fusion **40**, 175 (1998); M. H. Key *et al.,* Phys. Plasmas **5**, 1966 (1998); G. Pretzler *et al.,* Phys. Rev. E **58**, 1165 (1998); K. Krushelnick *et al.,* Phys. Rev. Lett. **83**, 737 (1999).